

Measurement of Two-Dimensional Binding Constants between Cell-Bound Major Histocompatibility Complex and Immobilized Antibodies with an Acoustic Biosensor

Michael Saitakis, Anastasia Dellaporta, and Electra Gizeli

Institute of Molecular Biology and Biotechnology, Foundation for Research and Technology Hellas, Vassilika Vouton, 71110 Heraklion, Crete, Greece, and Department of Biology, University of Crete, Vassilika Vouton, 71409 Heraklion, Crete, Greece

ABSTRACT Gaining insights into the dynamic processes of molecular interactions that mediate cell-substrate and cell-cell adhesion is of great significance in the understanding of numerous physiological processes driven by intercellular communication. Here, an acoustic-wave biosensor is used to study and characterize specific interactions between cell-bound membrane proteins and surface-immobilized ligands, using as a model system the binding of major histocompatibility complex class I HLA-A2 proteins to anti-HLA-A2 monoclonal antibodies. The energy of the acoustic signal, measured as amplitude change, was found to depend directly on the number of HLA-A2/antibody complexes formed on the device surface. Real-time acoustic data were used to monitor the surface binding of cell suspensions at a range of 6.0×10^4 to 6.0×10^5 cells mL^{-1} . Membrane interactions are governed by two-dimensional chemistry because of the molecules' confinement to the lipid bilayer. The two-dimensional kinetics and affinity constant of the HLA-A2/antibody interaction were calculated ($k_a = 1.15 \times 10^{-5} \mu\text{m}^2 \text{s}^{-1}$ per molecule, $k_d = 2.07 \times 10^{-5} \text{s}^{-1}$, and $K_A = 0.556 \mu\text{m}^2$ per molecule, at 25°C), based on a detailed acoustic data analysis. Results indicate that acoustic biosensors can emerge as a significant tool for probing and characterizing cell-membrane interactions in the immune system, and for fast and label-free screening of membrane molecules using whole cells.

INTRODUCTION

Membrane proteins have great biological and biotechnological significance. They comprise $\sim 30\%$ of all proteins encoded by the genome, and they mediate interactions of cells with extracellular components or other cells. They also comprise the target for the majority of drugs on the market. Under *in vivo* conditions, cells are in constant communication with their environment via molecules anchored to or embedded in the cell membrane. The binding of cell-membrane molecules to specific ligands that are also attached to another (cell) surface is pivotal in numerous physiological and developmental conditions, such as leukocyte adhesion and rolling (1–4) and cell-mediated immune reactions (5–7). Surface interactions involving cell-bound membrane proteins are physically distinct from the binding interactions that occur when soluble molecules are used, because membrane receptors are restricted in two dimensions due to spatial limitations imposed by the cell membrane. As a result, membrane-associated events are governed by two-dimensional (2D) kinetics and affinity (8), where association rate (k_a) and binding affinity (K_A) constants are expressed in $\mu\text{m}^2 \text{s}^{-1}$ per molecule and μm^2 per molecule, respectively (because these constants are proportional to the surface density commonly measured in molecules μm^{-2}), instead of the traditional three-dimensional (3D) chemistry that occurs between soluble molecules, with k_a in $\text{M}^{-1} \text{s}^{-1}$ and K_A in M^{-1} . The calculation of 2D binding

parameters offers a means to understand better the binding mechanisms of molecular interactions between apposed membranes, because these parameters are related directly to the function of membrane proteins (9–11).

The recent development of fluorescence and mechanical methods allowed a partial characterization of 2D membrane-protein interactions. Fluorescence methods were used to derive 2D binding affinities during the application of receptor-expressing cells on a glass-supported lipid bilayer reconstituted with fluorescently labeled ligands (9,11,12). The equilibrium constants for cell adhesion molecule CD2 and its ligands (9,11,12) CD48 and CD58, and for cell adhesion molecule CD28 and its ligand (13) CD80, were derived by fluorescence methods. Mechanical methods, such as the flow chamber assay (3,4,14), the micropipette method (15,16), and the centrifugation method (17), are based on the fact that two surfaces (e.g., cell-cell or cell-substrate) are cross-linked through the formation of receptor-ligand bonds. These techniques allow for the determination of 2D dissociation rate constants from measurements of the lifetime of single molecule-mediated adhesion. The dissociation rate constants for the ligand binding of L-selectin and P-selectin are among the parameters that were calculated by such methods (4,10). A combination of these methods could provide both 2D affinity and kinetics data. However, such an approach would be labor-intensive and not suitable for the development of fast or high-throughput assays. As a result, the development of tools for the real-time analysis of cell-bound interactions would be significant for both basic and applied research.

Biosensors are analytical devices that offer rapid detection of biological interactions occurring between surface-bound

Submitted February 25, 2008, and accepted for publication August 1, 2008.

Address reprint requests to Electra Gizeli, Institute of Molecular Biology and Biotechnology, Foundation for Research and Technology Hellas, Vassilika Vouton, 71110 Heraklion, Crete, Greece. E-mail: gizeli@imbb.forth.gr.

Editor: Arup Chakraborty.

© 2008 by the Biophysical Society
0006-3495/08/11/4963/09 \$2.00

doi: 10.1529/biophysj.108.132118

molecules and their water-soluble or dispersed analytes. They can also provide detailed information about binding affinity and, often, the kinetics of binding. Mass-related, label-free transduction technologies based on optical and acoustic waves were used extensively for the study of various interactions, i.e., antibody/antigen, protein/peptide, DNA/protein, and DNA/DNA (18,19). Despite the wide use of direct biosensors with soluble analytes, limited data exist on the detection of whole cells and cell-bound membrane-receptor interactions (20). Surface plasmon resonance (SPR) devices were successful in the detection of red blood cell-ligand interactions because of the deformable disk morphology of red blood cells, which facilitates coverage of the sensor surface (21,22). However, optical biosensors are less effective with spherical cells, probably because of the relatively large cell mass present in the ~ 300 -nm evanescent field, which produces a bulk response overshadowing the underlying mechanisms related to the formation of membrane receptor/ligand bonds (20).

Acoustic biosensors have the potential to study cell/substrate binding events because they are sensitive not only to mass coupling, but also to viscoelastic changes occurring close to the sensor surface (23). Studies based on a quartz-crystal microbalance device were used for monitoring macroscopic dynamic processes occurring close to the sensor surface. Such studies provided important information about different molecular mechanisms responsible for cell attachment, adhesion, spreading, and cytoskeleton rearrangement (24–26). However, these studies were all qualitative, and, to our knowledge, full characterization of cell-surface interactions has not been realized.

In this work, a shear acoustic-wave biosensor, based on a Love waveguide configuration, was used to monitor the binding of receptor-bearing cells, i.e., B-lymphoblastoid LG2 cells expressing class I major histocompatibility complex (MHC) molecules, to a specific monoclonal antibody immobilized on the sensor surface. Acoustic energy dissipation, detected as a function of time upon the addition of viable cells to a modified sensor surface, was found to correlate directly with the number of cell-membrane receptors specifically attached to immobilized antibodies. This finding, together with a detailed mathematical analysis of the binding, allowed for the kinetic and physicochemical characterization of interactions leading to the calculation of 2D kinetic and affinity parameters.

EXPERIMENTAL SECTION

Cell cultures and treatments

The Epstein-Barr virus-transformed human B-lymphoblastoid cell line LG2 (HLA-A*0201^{+/+}, kindly provided by H. Reyburn, Department of Pathology, University of Cambridge, Cambridge, UK) and chronic myelogenous leukemic K562 cells (HLA-A⁻B⁻C⁻, a generous gift of S. Perez, Center for Cancer Immunology and Immunotherapy, St. Savvas Hospital, Athens, Greece) were used in this work. RPMI-1640 (Invitrogen, Carlsbad, CA), supplemented with 1 mg L⁻¹ gentamycin and 10% fetal bovine serum, was used as culture medium. Culture flasks were kept in a humidified 5% CO₂ atmosphere at 37°C. The medium was exchanged every 2–3 days. Cell density was 3–8 × 10⁵ cells

mL⁻¹ in normal cultures, and 2–3 × 10⁶ cells mL⁻¹ in high-density cultures. Viability was checked before experiments by the trypan blue exclusion technique, and cell number was counted on a Neubauer slide. Dead cells never constituted over 5% of the total. Cells were washed with phosphate-buffered saline (PBS) (Sigma, St. Louis, MO), centrifuged at 250 × *g* and resuspended in PBS before addition to the sensor surface. To remove cell-surface HLA-A2-associated peptides, LG2 cells were briefly (90 s) treated with ice-cold citric acid-Na₂HPO₄ buffer at pH 3.2 (27) (a mixture of an equal volume of 0.263 M citric acid and 0.123 M Na₂HPO₄), and then washed with PBS.

Flow cytometry

For measuring the number of cell-surface HLA-A2 molecules, cells were incubated with the anti-HLA-A2 monoclonal antibody BB7.2 (Becton Dickinson, Franklin Lakes, NJ) and fluorescein isothiocyanate-conjugated anti-mouse IgG secondary fluorescence-activated cell sorter antibody (Dako, Glostrup, Denmark), both at saturating conditions. Samples were analyzed in a fluorescence-activated cell sorter (FACS) scanner (FACS Culiber, Becton Dickinson). Light-scattering and fluorescein isothiocyanate fluorescence data were collected on four-decade logarithmic scales. We used QIFIKIT (Dako) to perform a quantitative immunofluorescence indirect assay, using different populations of plastic beads with a known specific number of attached mouse immunoglobulin G (IgG) molecules. The number of cell-surface HLA-A2 molecules was calculated according to the manufacturer's instructions.

Acoustic device setup

The 110-MHz quartz devices were fabricated in-house on 0.5-mm-thick Y-cut piezoelectric quartz crystals. The interdigitated transducers, composed of a 210-nm-thick Cr/Au (10/200 nm) electrode, consisted of 80 pairs of split fingers, with a periodicity of 45 μm. The devices were coated with a 0.7-μm-thick poly(methylmethacrylate) (Aldrich, St. Louis, MO) layer, on top of which 20 nm of gold were sputtered, using a BAL-TEC SCD 050 sputter coater (BAL-TEC AG, Balzers, Liechtenstein). The acoustic devices were mounted on a special holder, and liquid was pumped through on the area between interdigitated transducers (IDTs), using a peristaltic pump (Gilson, Middleton, WI) and a flow-through cell. The flow cell was sealed on the surface by using a custom-made rubber gasket, exposing a sensing area of 12 mm². A Hewlett-Packard (Palo Alto, CA) 4195A network analyzer was used to monitor the amplitude and phase of the wave, and LabVIEW (National Instruments, Austin, TX) software was used for collecting acoustic data.

Preparation of biosensor surfaces and acoustic cell detection

Freshly plasma-etched gold surfaces were incubated with a protein G (Calbiochem, San Diego, CA) solution (1 mg mL⁻¹) that was left to adsorb for 1 h at room temperature. After protein adsorption, the devices were inserted in the device holder, washed, and left to equilibrate with PBS (Sigma) at a flow rate of 50 μL min⁻¹. Antibody solutions of 0.1, 0.5, 1, or 10 μg mL⁻¹ were pumped over the biosensor surfaces at a 25-μL min⁻¹ flow rate, and the interaction with gold-adsorbed protein G was monitored in real time. The IgG surface densities were measured with SPR (SR7000, Reichert Analytical Instruments, Depew, NY) by injecting the antibody over a protein G-modified sensor surface. Acoustic experiments with cell suspensions involved the addition of cell suspensions with cell numbers ranging from 6.0 × 10⁴ to 6.0 × 10⁵ cells mL⁻¹ on the device surface, at a flow rate of 10 μL min⁻¹. Experiments were run at least in triplicate. Real-time acoustic data were analyzed using Microcal (Northampton, MA) Origin 6.1 software.

Image acquisition

After an acoustic experiment, the biosensor surface was observed under a Nikon (Tokyo, Japan) Eclipse E800 microscope, and photographs were

taken with an attached Nikon Coolpix E5400 camera. Because the sensor chip is not opaque, no fluorescent staining was needed for the observation of cells. Image analysis was performed using Adobe Photoshop software. Cells on the sensor surface were counted in at least three different areas.

RESULTS AND DISCUSSION

Love-wave device and receptor/ligand pair

The acoustic waveguide device (Fig. 1), operating at 110 MHz, was described elsewhere (28–32). Briefly, the apparatus comprises a quartz-crystal device that uses a set of IDTs to generate and detect a shear-horizontal surface acoustic wave. The phase and amplitude of the wave, which are related to acoustic velocity and energy, respectively, are measured as a function of time through electrical connections to the IDTs. A polymer layer, deposited on the device surface, serves as an acoustic waveguide by localizing the acoustic energy of the wave close to the sensing surface. An additional gold layer, deposited on top of the polymer, serves as a surface that allows immobilization of the biorecognition layer. All sensing occurs only within the liquid layer in contact with the device surface, in which there is significant displacement as a result of acoustic wave/liquid coupling. The thickness of this layer, defined as the penetration depth (23) δ of the sensor, is a feature of the operating frequency f and interface viscosity η , according to $\delta = \sqrt{\eta\rho/2\pi f}$. The penetration depth of the 110-MHz sensor used in this study is calculated at 50 nm for pure water. In practice, calculating the exact viscosity of an interface layer when cells are bound to the device surface is not easy. However, indirect evidence suggests that the sensor's response during cell-binding is similar to that obtained when the device is loaded with 16% glycerol, corresponding to a penetration depth of ~ 100 nm.

The device was used to detect interactions between receptors attached to whole cells and antibodies immobilized on the sensor surface (Fig. 2). The membrane receptor used was the HLA-A2 molecule, the most common class I MHC allele in human populations, expressed in the B-lymphoblastoid LG2 cell line. The natural function of HLA-A2 is to

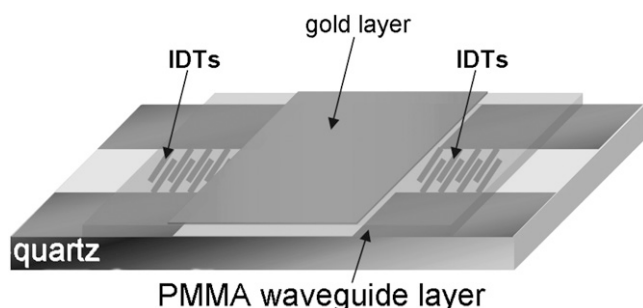


FIGURE 1 Schematic representation of acoustic Love-wave biosensor. Surface of quartz-based acoustic-wave device, where two IDTs are deposited, is covered with a thick polymer guiding layer. A thin layer of gold is deposited on top of the poly(methylmethacrylate) (PMMA) and between IDTs.

present short, endogenous peptides (8–11 residues) to the T-cell receptors of T lymphocytes, which can trigger an immune response (33). The surface-immobilized ligand was the anti-HLA-A2 monoclonal antibody BB7.2. Oriented immobilization of the antibody through the Fc fragment (31,34) was achieved by applying anti-HLA-A2 antibody to a protein G-coated device surface. The antibody is specific for the α chain (35) of HLA-A2 when the latter exists in a heterotrimer form consisting of α chain/ β_2 -microglobulin/peptide (36). Apart from the heterotrimeric form, HLA-A2 molecules on the cell membrane can be found in a heterodimeric form, i.e., simply as α -chain/ β_2 -microglobulin, or as single α -chains (37); α -chains in the last two forms are not recognized by BB7.2. The number of HLA-A2 heterotrimers present on the cell membrane was controlled by using LG2 cells prepared under three different conditions: as untreated cells, as mild acid-treated, and as untreated from high-density cultures. Mild acid treatment removes bound peptides from the HLA groove (27), so that treated cells have low heterotrimer numbers. In addition, cells grown in high-density cultures will display high heterotrimer numbers on the cell surface (37). Using an indirect quantitative immunofluorescence assay and flow cytometry, the number of HLA-A2 heterotrimers (also referred to here as HLA) on the cell surface was calculated. The values were: $3.7\text{--}5.7 \times 10^5$ HLA-A2 molecules per untreated LG2 cell (12 experiments), $1\text{--}10 \times 10^4$ HLA-A2 molecules per mild acid-treated LG2 cell (6 experiments), and $9.7\text{--}10.0 \times 10^5$ HLA-A2 per LG2 cell from a high-density culture (4 experiments).

Acoustic signal-damping as a measure of number of HLA/anti-HLA bonds

The Love-wave acoustic sensor is sensitive to mass-loading and viscosity changes occurring within the sensor's penetration depth (23). Mass changes because of the deposition of a rigid film will only affect the phase or frequency. Energy dissipation, measured here as amplitude change, will only be affected by viscosity/viscoelastic changes (23). Previous studies using shear acoustic-wave devices showed that dissipation is more sensitive to cell adhesion than phase or frequency/phase as a result of severe damping of the acoustic wave by the presence of viscoelastic cells (26,38). Here, the addition of LG2 cells to the modified biosensor surface affected the amplitude signal significantly and in proportion to the concentration of the injected cell suspension, i.e., cells mL^{-1} (see Fig. 6 a). In contrast, the phase signal could not discriminate between samples containing different number of cells (data not shown).

In addition, it was shown that the acoustic signal is mostly sensitive to specific cell/surface contacts, whereas the presence of the cell alone in the vicinity of the sensor surface is not sufficient to produce a signal change (24,39,40). To investigate further whether the signal change reflects the formation of cell-bound HLA/anti-HLA-A2 complexes, experiments were performed using cells with different numbers of HLA-A2

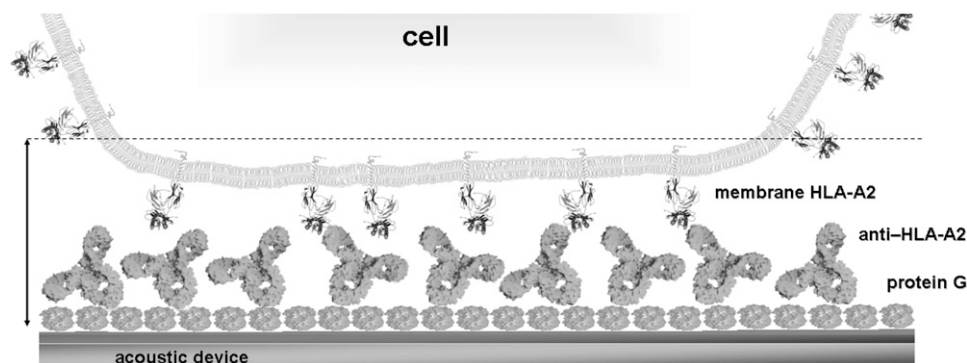


FIGURE 2 Schematic representation of biorecognition layer. Cells are attached to surface via specific bonds formed between cell-bound HLA-A2 molecules and surface-immobilized anti-HLA-A2 antibody. Dashed line indicates approximate area inside which the Love-wave acoustic biosensor is sensitive to interfacial changes (image not drawn to scale).

receptors on their surface. For this reason, the three different types of LG2 cells, i.e., untreated, treated with a mild acid, and from high-density cultures, were injected under flow ($10 \mu\text{L min}^{-1}$) at various concentrations on the antibody-modified surface. Parallel microscopic and acoustic monitoring of the number of bound cells and amplitude change, respectively, revealed that, for the same number of bound cells, the acoustic-signal change depended on the number of HLA-A2 molecules present on the cell membrane. This was clearly shown by plotting amplitude changes versus total number of HLA-A2 molecules available for binding on the sensor surface (Fig. 3); the number of HLA molecules was derived by multiplying the number of cells on the sensor surface at equilibrium by the corresponding number of HLA heterotrimers (determined by FACS). Fig. 3 proves that the formation of specific HLA/anti-HLA bonds is the major cause of the acoustic response, and not the immobilization of cells on the sensor surface per se.

A physical explanation of these observations can be derived by looking at the sensor/cell interface (Fig. 2). Close inspection of the geometry of the biological sensing layer reveals that protein G would form a 5–10-nm-thick layer, whereas the IgG layer is extended further, for another 15-nm maximum (41). Upon cell addition, the HLA molecules attached to the 6–10-nm-thick cell membrane would interact

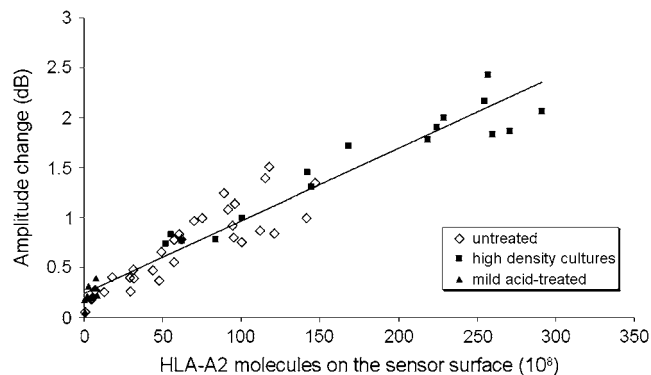


FIGURE 3 Amplitude-signal changes plotted against number of total membrane HLA-A2 molecules on sensor surface for three types of LG2 cells (untreated, high-density cultures, and mild acid-treated).

with the immobilized IgG through the 7-nm-long extracellular part of HLA-A2 molecules (33). Taking into account the sensor's penetration depth (~ 100 nm), it is clear that the vast majority of the cell mass (cell diameter, $14.4 \pm 2.2 \mu\text{m}$) will be outside the device's sensing volume. Our results suggest that the total mass of the HLA-A2 receptors bound to surface-immobilized antibodies is too low to cause a phase change that can be directly correlated to mass coupling. Instead, the amplitude response, which is related to acoustic energy dissipated from the sensor surface to the liquid interface, shows remarkable sensitivity. Apparently the cell membrane, in which HLA molecules are embedded, acts as an effective damper by absorbing energy through the HLA-A2/antibody bonds, and hence the observed amplitude change occurs.

The specificity of binding was assessed with acoustic experiments recording amplitude change during the addition of 2.5×10^5 cells/mL to the device surface. Cell samples included untreated K562 cells (which do not express any HLA-A2), untreated LG2 cells, and anti-HLA pretreated LG2 cells on the antibody-modified surface, as well as untreated LG2 cells on biosensor surfaces lacking the anti-HLA antibody, i.e., with just protein G. The LG2 cells pretreated with anti-HLA antibody showed lower binding than the untreated ones, because fewer HLA heterotrimers were available to bind to the immobilized antibody. Finally, negligible binding of LG2 cells to the protein G-modified surface was detected. These experiments proved the specificity of the observed signal change to the formation of HLA/anti-HLA bonds (Fig. 4).

Real-time acoustic experiments with cell suspensions under flow

The interactions of cell-membrane molecules with surface-immobilized ligands may not be affected solely by molecular kinetics and affinity if the binding takes place under an externally applied mechanical force (42) inducing high shear stresses, as is the case with mechanical methods used for determining 2D dissociation rate constants (3,4,14). Under conditions of flow, a critical number of cell-membrane receptor/immobilized ligand bonds must be formed for the attachment of a single cell (43,44). In this study, we wanted to

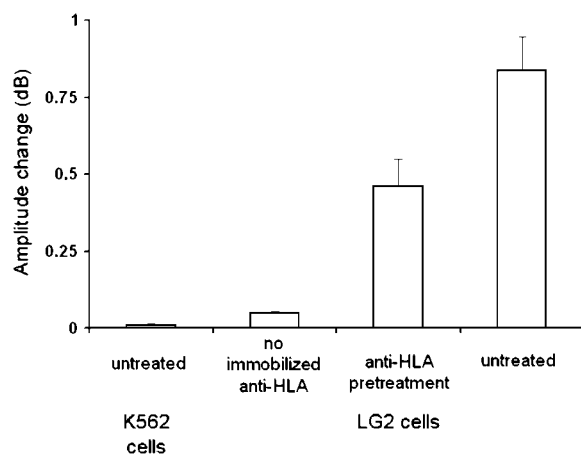


FIGURE 4 Specificity of cell binding assessed with amplitude signal change during addition of 2.5×10^5 cells mL^{-1} to the device surface. Cell samples included untreated K562 cells (which do not express any HLA-A2) on anti-HLA modified device surfaces, untreated LG2 cells on biosensor surfaces lacking the anti-HLA antibody, and anti-HLA pretreated and untreated LG2 cells on antibody-modified surfaces.

minimize the effect of external mechanical forces applied on cells, i.e., the shear stress, and only probe the molecular kinetics and affinity. Therefore, low flow rates were used so that the shear stress applied to cells inside the flow cell (31,45) (3.9×10^{-3} dynes cm^{-2}) would not induce cell detachment after initial tethering (4). The flow rate of $10 \mu\text{L min}^{-1}$ was selected for all experiments, because it yielded the highest acoustic signal change on addition of 2.5×10^5 cells mL^{-1} , indicating efficient cell transfer to the biosensor surface and the development of a sufficient number of stable HLA/anti-HLA bonds, leading to cell attachment.

In addition, a relatively high surface density ($5.9 \pm 1.9 \times 10^3$ molecules μm^{-2}) was used for the immobilized anti-HLA-A2, to facilitate cell attachment. Three lower surface densities were also applied (Table 1). It was found that the number of LG2 cells attached on the sensor surface per unit area is minimally affected by even a fivefold decrease in anti-HLA surface density. It should be also noted that the off-rate ($2.90 \times 10^{-4} \text{ s}^{-1}$) of the interaction between protein G and

TABLE 1 Effect of surface concentration of anti-HLA monoclonal antibody on acoustic signal amplitude change and number of bound cells during application of 2.5×10^5 cells mL^{-1}

Anti-HLA concentration ($\mu\text{g mL}^{-1}$)	Anti-HLA surface density (molecules μm^{-2})*	Amplitude change (dB) for 2.5×10^5 cells mL^{-1}	LG2 cells attached on sensor surface per $\text{mm}^{2\dagger}$
0.1	88	0.06	13
0.5	572	0.29	257
1.0	1181	0.84	1236
10.0	5858	0.99	1287

*Values obtained from surface plasmon resonance.

[†]Cells on sensor surface were counted under microscope from at least three different areas.

mouse monoclonal antibodies (31) is slower than the 30 min during which the signal of cell binding is monitored and used for kinetics. Thus, the higher anti-HLA surface density was selected for all acoustic experiments, because it also offered better reproducibility of the acoustic signal.

Fig. 5 shows a typical response of the acoustic-signal amplitude change as a function of time. After harvesting, LG2 cells in PBS were injected over the antibody-functionalized sensor surface under flow ($10 \mu\text{L min}^{-1}$). Before and after the injection of cells, the acoustic signal was equilibrated with PBS as running buffer, at a flow rate of $50 \mu\text{L min}^{-1}$. Furthermore, to minimize any interference from cell diffusion-limited kinetics, only that part of the graph that fitted well (95%) to a single exponential curve, assuming a one-to-one reaction, was applied to our calculations (46), whereas the first 500 s after the addition of cells were not included in the kinetic analysis. Cells come into contact with the sensor surface via their microvilli, and initial contacts are formed between surface-immobilized IgG and HLA molecules at the tips of the microvilli. Cells, in general, spread isotropically in the absence of serum proteins (47), and at high densities of immobilized ligand (48). Thus, LG2 cells will form a large, circular contact area during the first minutes of interaction (49). This contact area will be discontinuous, and will be formed by spatially separated point contacts (microvilli). After this initial phase (first 500 s), the signal changes observed should mainly reflect the formation of new HLA/antibody bonds as a result of the spreading of microvilli and HLA-A2 lateral diffusion in the cell-surface contact area. Over time, the microvilli will spread to form a flat contact area (8,11). The time required for cells to reach equilibrium was 62 ± 18 min (25 experiments from eight different concentrations). Microscopy photographs revealed that, at equilibrium, LG2 cells retain their round shape on the biosensor surface and display limited spreading, mediated by short filopodia (Fig. 5, *inset*).

2D kinetic analysis of cell-bound HLA-A2/anti-HLA interaction

The amplitude signal change is a measure for the formation of HLA-IgG bonds. Thus, kinetic information can be calculated from the real-time binding curves for cell-bound HLA/immobilized anti-HLA interactions. Experiments were performed with cell suspensions containing different numbers of untreated LG2 cells (Fig. 6 *a*). For kinetic calculations, the analysis described for 3D interactions (31,50) was applied according to the equation

$$\Delta(dA/dt)/\Delta A = k_a C + k_d, \quad (1)$$

where $\Delta(dA/dt)$ and ΔA represent the change in rate and overall amplitude, respectively, derived from real-time graphs, C represents the concentration of soluble analyte, and k_a and k_d represent the association and dissociation rate

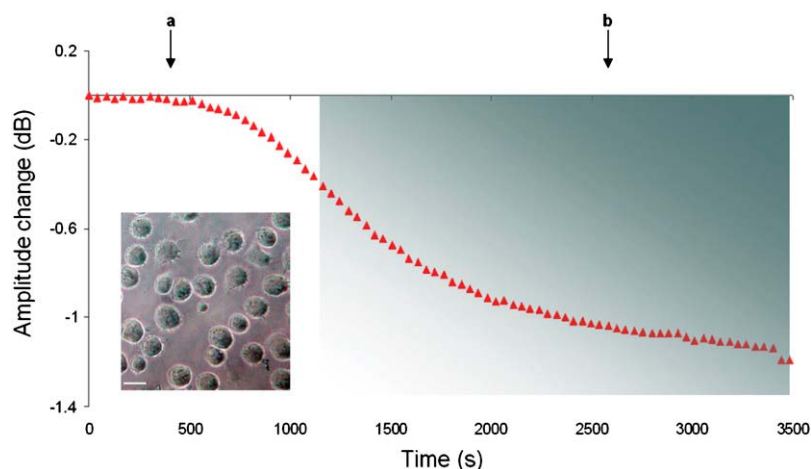


FIGURE 5 Amplitude change as a function of time during interaction of LG2 cells (2.5×10^5 cells mL^{-1}) with surface-immobilized anti-HLA antibody. Arrows (*a* and *b*) indicate corresponding times for addition of cell suspension and buffer, respectively. The binding curve is divided into two phases. The first (~ 500 s after addition) represents time required for cells to reach the surface and form initial tethers, and is cell-diffusion limited. The second phase (*colored rectangle*) depicts formation of HLA/anti-HLA bonds. (*Inset*) Microscopy photograph of LG2 cells on biosensor surface after an acoustic experiment. Scale bar, $15 \mu\text{m}$.

constants, respectively. In our case, the 3D molar concentration C was replaced by the 2D HLA-A2 surface density C^{2D} , which should reflect the number of cell-membrane HLA molecules available for binding, and k_a and k_d are the corresponding 2D rate constants.

For determining C^{2D} , two parameters are of interest: 1), the total number of laterally mobile HLA molecules available for interaction on each cell surface, i.e., [HLA] and 2), the total number of bound cells or % surface coverage by cells. The number of laterally mobile HLA molecules available for interactions on each cell surface is given as (12)

$$[\text{HLA}] = N_{\text{HLA}} \times (f/S_{\text{cell}}). \quad (2)$$

N_{HLA} is the total number of HLA molecules on the cell surface, f is their fractional mobility, and S_{cell} is the cell surface. The surface area (S_{cell}) of cells was calculated at $633.15 \mu\text{m}^2$ ($S_{\text{cell}} = \pi d^2$, where the cell's diameter d was measured from microscopy photos at $14.4 \mu\text{m}$). To account for the irregularities of the cell membrane (12), S_{cell} was multiplied by a surface roughness factor of 1.8, resulting in a final value of $1172.6 \mu\text{m}^2$. Based on the average number of 4.7×10^5 HLA-A2 receptors per untreated cell and the receptors' fractional mobility (51) f of 93.5%, [HLA] was calculated at 374 ± 80 molecules μm^{-2} . Because the experiments were run in the absence of culture medium and serum, we assume that there was no net change in the number

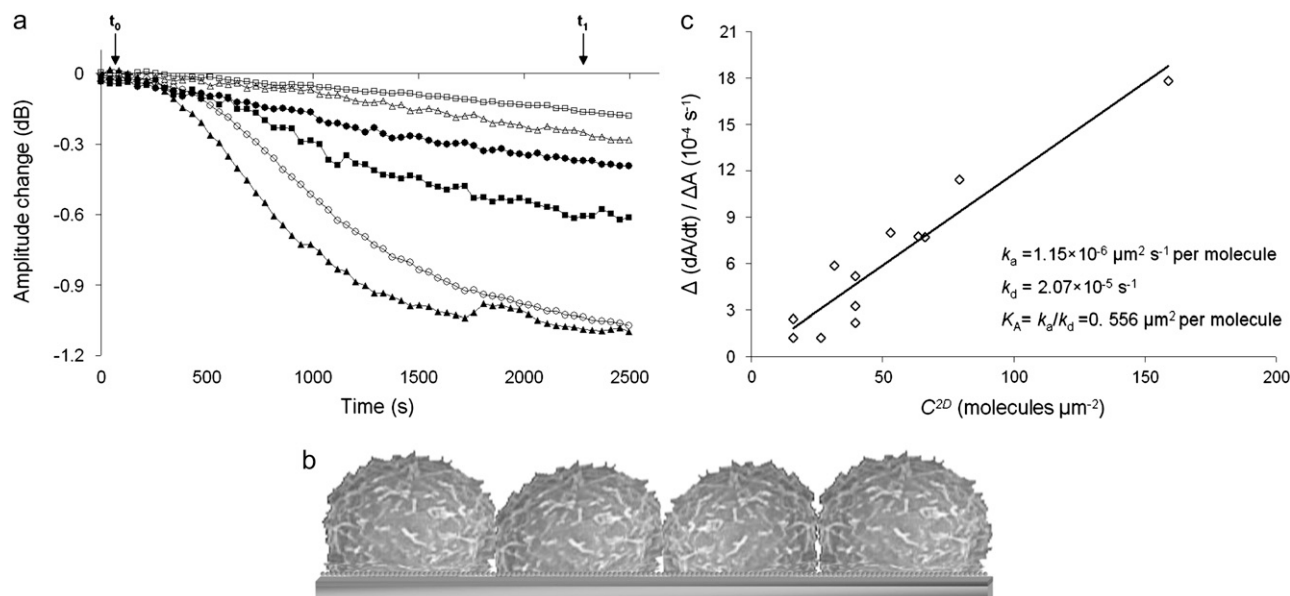


FIGURE 6 Kinetic analysis of cell-bound HLA/anti-HLA interaction. (*a*) Real-time binding curves when various LG2 cell suspensions were added over immobilized anti-HLA antibody. Arrows (t_0 and t_1) indicate times for addition of cell suspension and buffer, respectively. Cell suspensions: $6.0 \times 10^4/\text{mL}$ (\square), $1.2 \times 10^5/\text{mL}$ (Δ), $1.5 \times 10^5/\text{mL}$ (\bullet), $2.4 \times 10^5/\text{mL}$ (\blacksquare), $3.0 \times 10^5/\text{mL}$ (\circ), and $6.0 \times 10^5/\text{mL}$ (\blacktriangle). Note that only data used in the kinetic analysis are shown. (*b*) Schematic representation of sensor surface at full cell coverage $C_{\text{full}}^{\text{cells}}$. (*c*) Plot of $\Delta(dA/dt)/\Delta A$ (where (dA/dt) and ΔA are the rate and corresponding amplitude change derived from real-time curves, and $\Delta(dA/dt)/\Delta A$ is the slope of (dA/dt) against ΔA) versus effective [HLA], i.e., C^{2D} , as calculated from Eq. 4.

of HLA molecules on the cell surface, and also that the overall cell surface remained constant. Therefore, [HLA] was considered constant throughout the experiments.

The second parameter of interest was the % surface coverage by cells. In our experiments, the total number of HLA receptors per cell remained constant, and the only variable was the number of applied cells. This implies that 374 molecules μm^{-2} is the maximum [HLA] that can be presented to the sensor's surface and will correspond to the ideal case of complete coverage of the surface by cells, resulting in an almost flat membrane film apposed to the sensor's surface (Fig. 6 b). If $C_{\text{full}}^{\text{cells}}$ is the cell suspension at which full surface coverage is observed, then for cell suspensions lower than $C_{\text{full}}^{\text{cells}}$, the HLA surface density per cell will still remain 374 molecules μm^{-2} . However, the effective [HLA] sensed by the sensor will be a function of the coverage of the sensor surface by the cells, i.e., of $d_i^{\text{cells}}/d_{\text{full}}^{\text{cells}}$, where d is the cells' surface density on the device. The observed linear relationship between C_{cells} and d_{cells} up to the saturation level allows rewriting the above ratio as $C_i^{\text{cells}}/C_{\text{full}}^{\text{cells}}$.

Given the above analysis, C^{2D} , which is the effective [HLA] sensed by the sensor and, thus, the equivalent to the soluble analyte concentration used in Eq. 1, can be calculated as

$$C^{2D} = [\text{HLA}] \times C_i^{\text{cells}} / C_{\text{full}}^{\text{cells}}. \quad (3)$$

In our experiments, maximum cell coverage was observed at cell suspensions equal to or higher than $C_{\text{max}}^{\text{cells}} = 6 \times 10^5$ cells mL^{-1} , as detected acoustically through ΔA measurements. Microscopy photographs, obtained in parallel, revealed that the corresponding $d_{\text{full}}^{\text{cells}}$ (2603 cells mm^{-2}) was not equal to $d_{\text{full}}^{\text{cells}}$ but, in fact, corresponded to a surface coverage of 42.4% (Based on microscopy photos, after the experiments with cell suspensions of 6×10^5 cells mL^{-1} or higher, the observed maximum number of cells on the sensor surface was 31,236 cells. Taking into account the cell's maximum contact area ($162.9 \mu\text{m}^2$) and the sensor surface (12mm^2), the observed maximum coverage was calculated from the ratio of the total area covered by the cells versus the sensor surface, and was 42.4%.) This correction factor was finally taken into account when calculating C^{2D} . Therefore, Eq. 3 becomes

$$C^{2D} = 374 \times 0.424 \times C_i^{\text{cells}} / C_{\text{full}}^{\text{cells}} = 158.6 \times C_i^{\text{cells}} / C_{\text{full}}^{\text{cells}}. \quad (4)$$

Plotting $\Delta(dA/dt)/\Delta A$ (Eq. 1) versus C^{2D} (Eq. 4) allows for the measurement of the 2D association and dissociation rate constants: k_a from the slope and k_d from the intercept with the ordinate are calculated to be $1.15 \times 10^{-5} \mu\text{m}^2 \text{s}^{-1}$ per molecule and $2.07 \times 10^{-5} \text{s}^{-1}$, respectively (Fig. 6 c). The 2D binding affinity K_A is then calculated as $K_A = k_a/k_d = 0.556 \mu\text{m}^2$ per molecule.

The above analysis was performed given a constant surface density for immobilized IgG. Although dissociation was not observed for whole cells, it can occur for single HLA/anti-HLA bonds. Rebinding of dissociated HLA can readily

occur, given the relatively high surface antibody density ($5.9 \pm 1.9 \times 10^3$ molecules μm^{-2}). Moreover, the lateral diffusion of HLA molecules on the membrane of B-lymphoblastoid cells was higher (51) ($1.75 \times 10^{-1} \mu\text{m}^2 \text{s}^{-1}$) than the measured association rate constant for bond formation ($1.15 \times 10^{-5} \mu\text{m}^2 \text{s}^{-1}$). Hence the rate constant was the limiting step, and was therefore what was measured.

It is worth mentioning that the 2D binding parameters are not absolute. Affinity in two dimensions depends on the local microtopological conditions of the cell-substrate or cell-cell contacts (8,52). Molecular motion, membrane stiffness, cytoskeleton condition, and molecule segregation by size can all have an important effect on 2D interactions. In our case, the binding kinetics should also depend on the kinetics of membrane bending during the microvilli spreading process. Further experiments, e.g., with cytoskeleton tampering drugs, would shed more light on the individual contributions of each parameter.

Other 2D affinities were calculated using fluorescence methods (9,11,12) for interactions of the cell-adhesion molecule CD2 with its ligands, CD58 ($K_A = 0.13 \mu\text{m}^2$ per molecule) and CD48 ($K_A = 0.02 \mu\text{m}^2$ per molecule), attached to a planar lipid bilayer. For cell membrane-molecule interactions, there is a linear correlation between 3D and 2D binding affinities (8,53). The 2D affinities measured in the above systems are related to their low 3D affinities ($5 \times 10^5 \text{M}^{-1}$ and $4 \times 10^4 \text{M}^{-1}$, respectively). In our case, the 3D affinity was expected to be on the order of 10^8M^{-1} (as an antibody/antigen interaction). Therefore, a higher 2D binding affinity was measured ($0.556 \mu\text{m}^2$ per molecule).

CONCLUSIONS

We have developed what we consider a new and simple approach for detecting and characterizing whole-cell receptors interacting with surface-immobilized ligands. The acoustic signal used here, together with a modified 3D kinetic analysis, measured detailed 2D kinetics and derived both association and dissociation rate constants, as well as the affinity of cell-membrane protein binding events. Attempts to repeat this work with an SPR device were not successful. The change in refractive index observed upon cell addition was indiscriminate of specific or nonspecific binding, confirming that SPR gives a bulk response based on the cell mass present in the evanescent field, rather than on the number of specific cell/surface bonds. In contrast, the sensitivity of acoustic damping to the number of cell/surface specific bonds provides a unique sensing mechanism for investigating membrane interactions. Clearly, the proposed label-free and noninvasive acoustic biosensor could be applied further to characterize various membrane-associated events. Potential systems for study include T-cell receptor/MHC and MHC/antigenic peptide interactions using whole cells, without the need for membrane protein purification or reconstitution. Moreover, the technique resembles currently applied fluorescence methods, because it

measures unstressed molecular affinities between cell and substrate, while offering the advantage of yielding both kinetics and affinity constants without the need for labels. Using kinetic parameters for the calculation of 2D affinity constants also omits the need to measure contact areas between cell and substrate. Further advances in microfluidics will allow for the development of acoustic arrays that could facilitate drug screening during the simultaneous testing of large numbers of membrane-active compounds.

E.G. and A.D. thank Dr. S. Perez and Dr. A. Grizapis (St. Savvas Hospital, Athens, Greece) for help with initial cell cultures and antibody production. We are grateful to Prof. I. Athanassakis (Department of Biology, University of Crete) for providing access to the cell culture room, and Dr. I. Chatzidakis (Institute of Molecular Biology and Biotechnology, Foundation for Research and Technology Hellas) for help with FACS. We acknowledge Prof. C. Duschl for helpful discussions regarding the kinetic analysis.

The financial support of the Greek Secretariat of Research and Technology is acknowledged. The financial support of the Human Frontier Science Program is also acknowledged.

REFERENCES

- Juliano, R. L. 1987. Membrane receptors for extracellular matrix macromolecules: relationship to cell adhesion and tumor metastasis. *Biochim. Biophys. Acta.* 907:261–278.
- Berg, E. L., L. A. Goldstein, M. A. Jutila, M. Nakache, L. J. Picker, P. R. Streeter, N. W. Wu, D. Zhou, and E. C. Butcher. 1989. Homing receptors and vascular addressins: cell adhesion molecules that direct lymphocyte traffic. *Immunol. Rev.* 108:5–18.
- Alon, R., D. A. Hammer, and T. A. Springer. 1995. Lifetime of the P-selectin-carbohydrate bond and its response to tensile force in hydrodynamic flow. *Nature.* 374:539–542.
- Chen, S., and T. A. Springer. 2001. Selectin receptor-ligand bonds: formation limited by shear rate and dissociation governed by the Bell model. *Proc. Natl. Acad. Sci. USA.* 98:950–955.
- Springer, T. A. 1990. Adhesion receptors of the immune system. *Nature.* 346:425–434.
- Huppa, J. B., and M. M. Davis. 2003. T-cell-antigen recognition and the immunological synapse. *Nat. Rev. Immunol.* 3:973–983.
- van der Merwe, P. A., and S. J. Davis. 2003. Molecular interactions mediating T cell antigen recognition. *Annu. Rev. Immunol.* 21:659–684.
- Dustin, M. L., S. K. Bromley, M. M. Davis, and C. Zhu. 2001. Identification of self through two-dimensional chemistry and synapses. *Annu. Rev. Cell Dev. Biol.* 17:133–157.
- Dustin, M. L., L. M. Ferguson, P. Y. Chan, T. A. Springer, and D. E. Golan. 1996. Visualization of CD2 interaction with LFA-3 and determination of the two-dimensional dissociation constant for adhesion receptors in a contact area. *J. Cell Biol.* 132:465–474.
- Alon, R., S. Chen, K. D. Puri, E. B. Finger, and T. A. Springer. 1997. The kinetics of L-selectin tethers and the mechanics of selectin-mediated rolling. *J. Cell Biol.* 138:1169–1180.
- Dustin, M. L., D. E. Golan, D. M. Zhu, J. M. Miller, W. Meier, E. A. Davies, and P. A. van der Merwe. 1997. Low affinity interaction of human or rat T cell adhesion molecule CD2 with its ligand aligns adhering membranes to achieve high physiological affinity. *J. Biol. Chem.* 272:30889–30898.
- Zhu, D. M., M. L. Dustin, C. W. Cairo, and D. E. Golan. 2007. Analysis of two-dimensional dissociation constant of laterally mobile cell adhesion molecules. *Biophys. J.* 92:1022–1034.
- Bromley, S. K., A. Iaboni, S. J. Davis, A. Whitty, J. M. Green, A. S. Shaw, A. Weiss, and M. L. Dustin. 2001. The immunological synapse and CD28–CD80 interactions. *Nat. Immunol.* 2:1159–1166.
- Swift, D. G., R. G. Posner, and D. A. Hammer. 1998. Kinetics of adhesion of IgE-sensitized rat basophilic leukemia cells to surface-immobilized antigen in Couette flow. *Biophys. J.* 75:2597–2611.
- Chesla, S. E., P. Selvaraj, and C. Zhu. 1998. Measuring two-dimensional receptor-ligand binding kinetics by micropipette. *Biophys. J.* 75:1553–1572.
- Williams, T. E., S. Nagarajan, P. Selvaraj, and C. Zhu. 2001. Quantifying the impact of membrane microtopology on effective two-dimensional affinity. *J. Biol. Chem.* 276:13283–13288.
- Piper, J. W., R. A. Swerlick, and C. Zhu. 1998. Determining force dependence of two-dimensional receptor-ligand binding affinity by centrifugation. *Biophys. J.* 74:492–513.
- Gizeli, E., and C. R. Lowe. 2002. Biomolecular Sensors. Taylor & Francis, Inc., London.
- Cooper, M. A. 2003. Label-free screening of bio-molecular interactions. *Anal. Bioanal. Chem.* 377:834–842.
- Cooper, M. A. 2004. Advances in membrane receptor screening and analysis. *J. Mol. Recognit.* 17:286–315.
- Li, B., J. Chen, and M. Long. 2008. Measuring binding kinetics of surface-bound molecules using the surface plasmon resonance technique. *Anal. Biochem.* 377:195–201.
- Quinn, J. G., and R. O’Kennedy. 2001. Biosensor-based estimation of kinetic and equilibrium constants. *Anal. Biochem.* 290:36–46.
- Ballantine, D. S., R. M. White, S. J. Martin, A. J. Ricco, E. T. Zellers, G. C. Frye, and H. Wohltjen. 1997. Acoustic Wave Sensors. Academic Press, San Diego.
- Wegener, J., A. Janshoff, and H. J. Galla. 1998. Cell adhesion monitoring using a quartz crystal microbalance: comparative analysis of different mammalian cell lines. *Eur. Biophys. J.* 28:26–37.
- Galli Marxer, C., M. Collaud Coen, T. Greber, U. F. Greber, and L. Schlapbach. 2003. Cell spreading on quartz crystal microbalance elicits positive frequency shifts indicative of viscosity changes. *Anal. Bioanal. Chem.* 377:578–586.
- Li, J., C. Thielemann, U. Reuning, and D. Johannsmann. 2005. Monitoring of integrin-mediated adhesion of human ovarian cancer cells to model protein surfaces by quartz crystal resonators: evaluation in the impedance analysis mode. *Biosens. Bioelectron.* 20:1333–1340.
- van der Burg, S. H., E. Ras, J. W. Drijfhout, W. E. Benckhuijsen, A. J. Bremers, C. J. Melief, and W. M. Kast. 1995. An HLA class I peptide-binding assay based on competition for binding to class I molecules on intact human B cells. Identification of conserved HIV-1 polymerase peptides binding to HLA-A*0301. *Hum. Immunol.* 44:189–198.
- Gizeli, E. 2000. Study of the sensitivity of the acoustic waveguide sensor. *Anal. Chem.* 72:5967–5972.
- Gizeli, E., M. Liley, C. R. Lowe, and H. Vogel. 1997. Antibody binding to a functionalized supported lipid layer: a direct acoustic immunosensor. *Anal. Chem.* 69:4808–4813.
- Gizeli, E., F. Bender, A. Rasmusson, K. Saha, F. Josse, and R. Cernosek. 2003. Sensitivity of the acoustic waveguide biosensor to protein binding as a function of the waveguide properties. *Biosens. Bioelectron.* 18:1399–1406.
- Saha, K., F. Bender, and E. Gizeli. 2003. Comparative study of IgG binding to proteins G and A: nonequilibrium kinetic and binding constant determination with the acoustic waveguide device. *Anal. Chem.* 75:835–842.
- Tsartos, A., G. Papadakis, K. Mitsakakis, K. A. Melzak, and E. Gizeli. 2008. Quantitative determination of size and shape of surface-bound DNA using an acoustic wave sensor. *Biophys. J.* 94:2706–2715.
- Bjorkman, P. J., M. A. Saper, B. Samraoui, W. S. Bennett, J. L. Strominger, and D. C. Wiley. 1987. Structure of the human class I histocompatibility antigen, HLA-A2. *Nature.* 329:506–512.
- Fahnestock, S. R., P. Alexander, J. Nagle, and D. Filpula. 1986. Gene for an immunoglobulin-binding protein from a group G streptococcus. *J. Bacteriol.* 167:870–880.
- Parham, P., and F. M. Brodsky. 1981. Partial purification and some properties of BB7.2. A cytotoxic monoclonal antibody with speci-

- ficity for HLA-A2 and a variant of HLA-A28. *Hum. Immunol.* 3:277–299.
36. Hogan, K. T., and S. L. Brown. 1992. Localization and characterization of serologic epitopes on HLA-A2. *Hum. Immunol.* 33:185–192.
37. Matko, J., Y. Bushkin, T. Wei, and M. Edidin. 1994. Clustering of class I HLA molecules on the surfaces of activated and transformed human cells. *J. Immunol.* 152:3353–3360.
38. Janshoff, A., J. Wegener, M. Sieber, and H. J. Galla. 1996. Double-mode impedance analysis of epithelial cell monolayers cultured on shear wave resonators. *Eur. Biophys. J.* 25:93–103.
39. Wegener, J., J. Seebach, A. Janshoff, and H. J. Galla. 2000. Analysis of the composite response of shear wave resonators to the attachment of mammalian cells. *Biophys. J.* 78:2821–2833.
40. Hong, S., E. Ergezen, R. Lec, and K. A. Barbee. 2006. Real-time analysis of cell-surface adhesive interactions using thickness shear mode resonator. *Biomaterials.* 27:5813–5820.
41. Harris, L. J., S. B. Larson, K. W. Hasel, and A. McPherson. 1997. Refined structure of an intact IgG2a monoclonal antibody. *Biochemistry.* 36:1581–1597.
42. Hubble, J. 1997. Affinity cell separations: problems and prospects. *Trends Biotechnol.* 15:249–255.
43. Hammer, D. A., and D. A. Lauffenburger. 1987. A dynamical model for receptor-mediated cell adhesion to surfaces. *Biophys. J.* 52:475–487.
44. Chang, K. C., and D. A. Hammer. 1999. The forward rate of binding of surface-tethered reactants: effect of relative motion between two surfaces. *Biophys. J.* 76:1280–1292.
45. Lawrence, M. B., L. V. McIntire, and S. G. Eskin. 1987. Effect of flow on polymorphonuclear leukocyte/endothelial cell adhesion. *Blood.* 70:1284–1290.
46. Duschl, C., A. F. Sevin-Landais, and H. Vogel. 1996. Surface engineering: optimization of antigen presentation in self-assembled monolayers. *Biophys. J.* 70:1985–1995.
47. Dubin-Thaler, B. J., G. Giannone, H. G. Dobreiner, and M. P. Sheetz. 2004. Nanometer analysis of cell spreading on matrix-coated surfaces reveals two distinct cell states and STEPs. *Biophys. J.* 86:1794–1806.
48. Reinhart-King, C. A., M. Dembo, and D. A. Hammer. 2005. The dynamics and mechanics of endothelial cell spreading. *Biophys. J.* 89:676–689.
49. Cuvelier, D., M. Thery, Y. S. Chu, S. Dufour, J. P. Thiery, M. Bornens, P. Nassoy, and L. Mahadevan. 2007. The universal dynamics of cell spreading. *Curr. Biol.* 17:694–699.
50. Karlsson, R., A. Michaelsson, and L. Mattsson. 1991. Kinetic analysis of monoclonal antibody-antigen interactions with a new biosensor based analytical system. *J. Immunol. Methods.* 145:229–240.
51. Bierer, B. E., S. H. Herrmann, C. S. Brown, S. J. Burakoff, and D. E. Golan. 1987. Lateral mobility of class I histocompatibility antigens in B lymphoblastoid cell membranes: modulation by cross-linking and effect of cell density. *J. Cell Biol.* 105:1147–1152.
52. Shaw, A. S., and M. L. Dustin. 1997. Making the T cell receptor go the distance: a topological view of T cell activation. *Immunity.* 6:361–369.
53. Bell, G. I., M. Dembo, and P. Bongrand. 1984. Cell adhesion. Competition between nonspecific repulsion and specific bonding. *Biophys. J.* 45:1051–1064.